Supplementary Material for "Dual Topological Features of Weyl Semimetallic Phases in Tetradymite $BiSbTe_3$"

Z. Z. Zhou(周宇桢)[1], H. J. Liu(刘惠军)[2], G. Y. Wang(王国玉)[3], R. Wang(王锐)[1,*], and X. Y. Zhou(周小元) [1,†]

[1]*Center for Quantum Materials and Devices, College of Physics, Chongqing University, Chongqing 401331, China*

[2]*Key Laboratory of Artificial Micro- and Nano-Structures of Ministry of Education and School of Physics and Technology, Wuhan University, Wuhan 430072, China*

[3]*Chongqing Institute of Green and Intelligent Technology, Chinese Academy of Science, Chongqing 400714, China*

1. The electronic band structures of the $BiSbTe_3$ calculated by DFT and Wannier interpolation technique

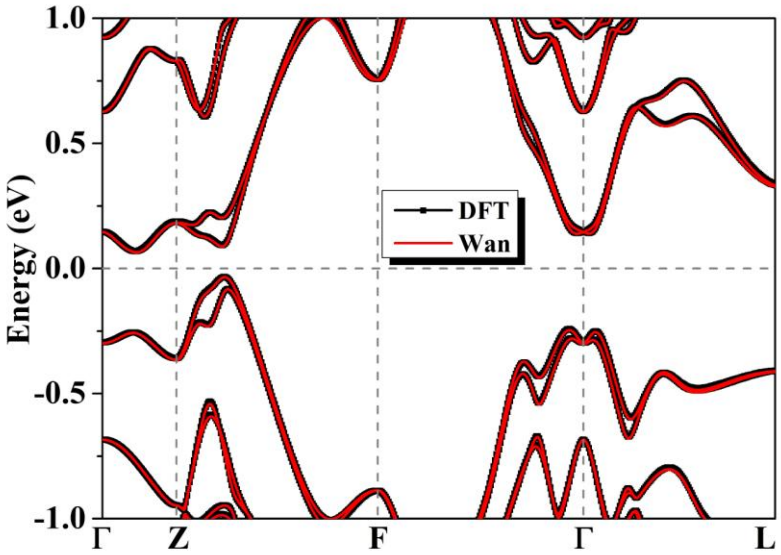

Figure S1. The DFT calculated band structure as compared with that obtained via Wannier interpolation technique. The results agree very well with each other, suggesting the reliability of Wannierization.

[*]Author to whom correspondence should be addressed. Email: rcwang@cqu.edu.cn

[†]Author to whom correspondence should be addressed. Email: xiaoyuan2013@cqu.edu.cn

2. The band structures of the $BiSbTe_3$ calculated by PBE and GW_0

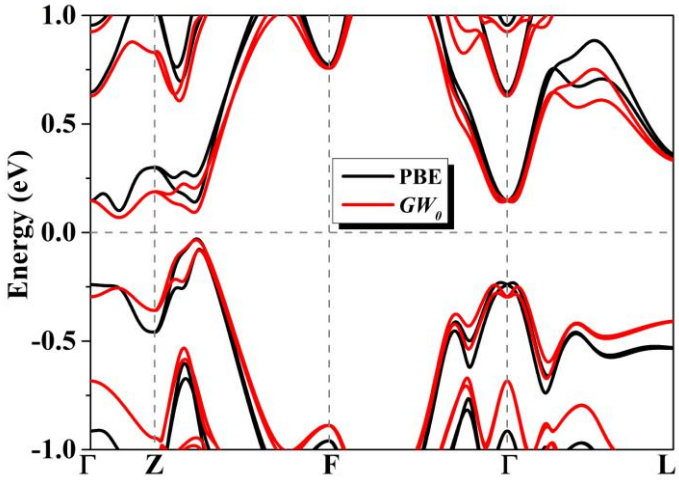

Figure S2. Calculated band structures of $BiSbTe_3$. Black and red lines correspond to the calculations with PBE+optB86b-vdW+SOC and PBE+GW_0+optB86b-vdW+SOC, respectively. The topological features of $BiSbTe_3$ are not affected by considering the GW_0 approximation, whereas the coordinates of band crossed points are slightly different from the PBE calculated results.

3. Recalculated results via MBJ method

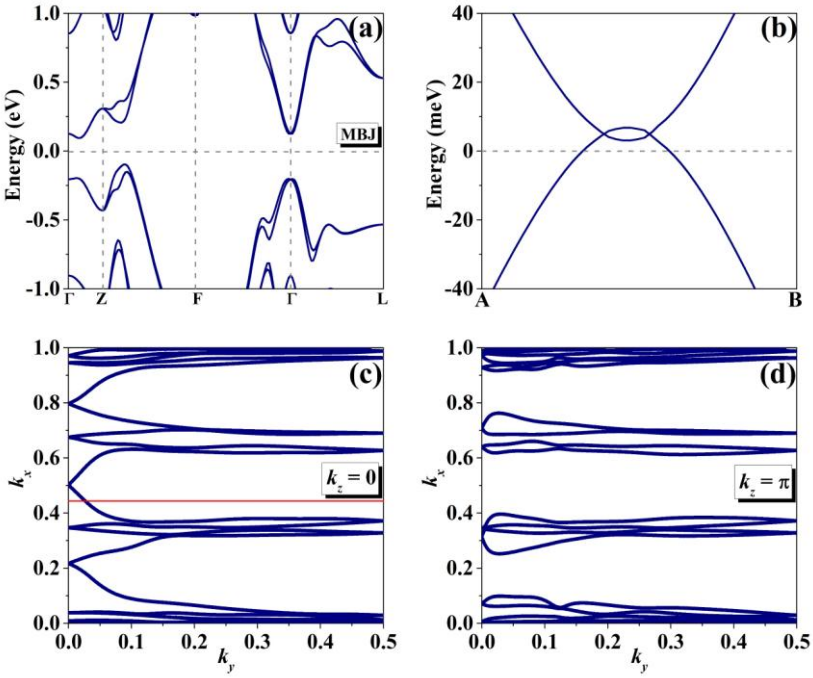

Figure S3. The MBJ calculated band structures along (a) high-symmetry lines and (b) specific line containing two Weyl points. Calculated evolution lines of Wannier centers in (c) $\boldsymbol{k_z} = 0$ and (d) $\boldsymbol{k_z} = \pi$ planes.

We have employed MBJ method to recalculate the band structures and recheck the topological states. The MBJ calculated band structures uncover the same band topology to that calculated from GW_0 method, including the distributions of Weyl points and Z2 topological invariants, as shown Fig. R1. Therefore, all these results confirm the reliability of our calculated results.

4. The phonon dispersion relations of $BiSbTe_3$

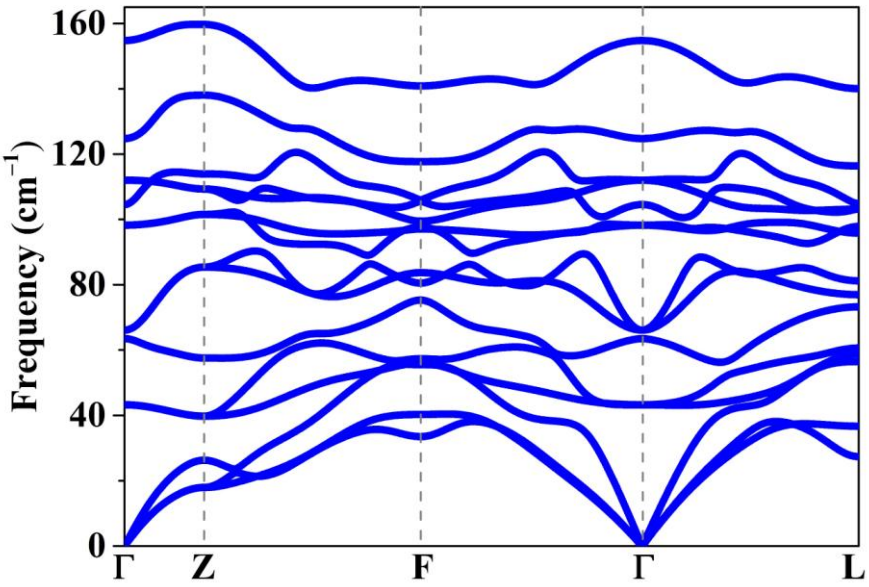

Figure S4. Calculated phonon dispersion relations of $BiSbTe_3$ based on the density functional perturbation theory.

5. The evolution lines of Wannier centers for tetradymite $BiSbTe_3$

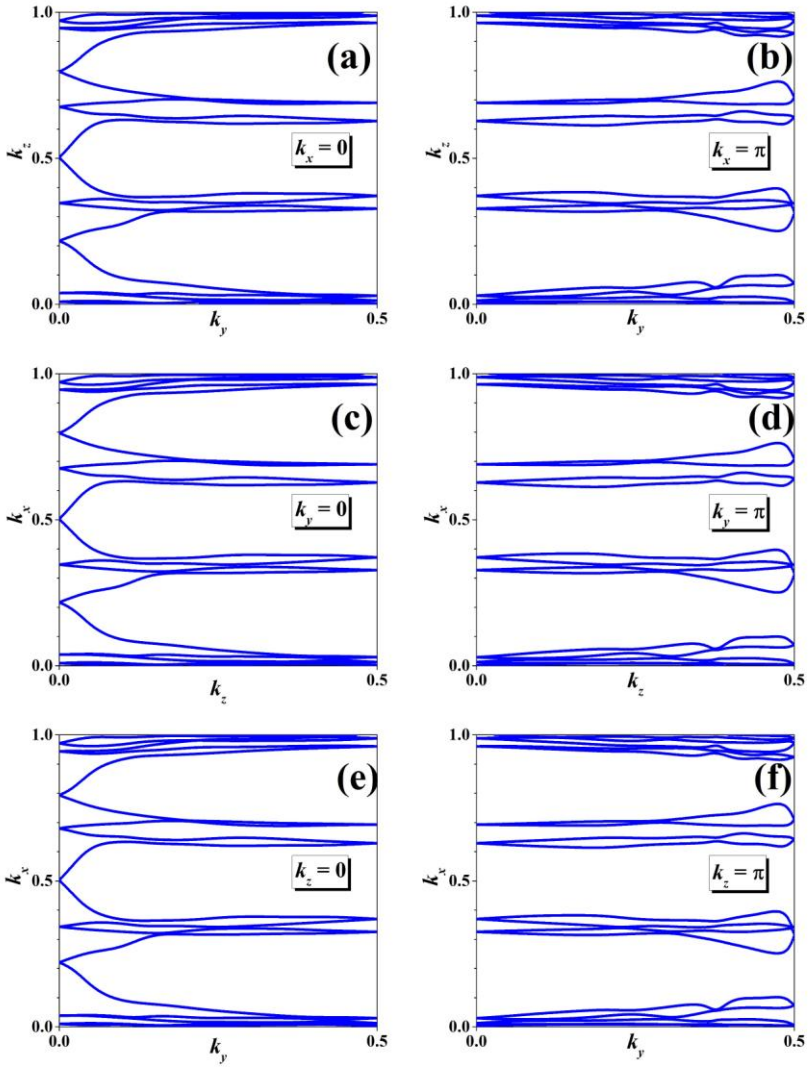

Figure S5. (a)~(f) Calculated evolution lines of Wannier centers in $\boldsymbol{k_x} = 0$, $\boldsymbol{k_x} = \pi$, $\boldsymbol{k_y} = 0$, $\boldsymbol{k_y} = \pi$, $\boldsymbol{k_z} = 0$, and $\boldsymbol{k_z} = \pi$ planes.

6. The graphical representation of the distribution of the symmetry protected Weyl points

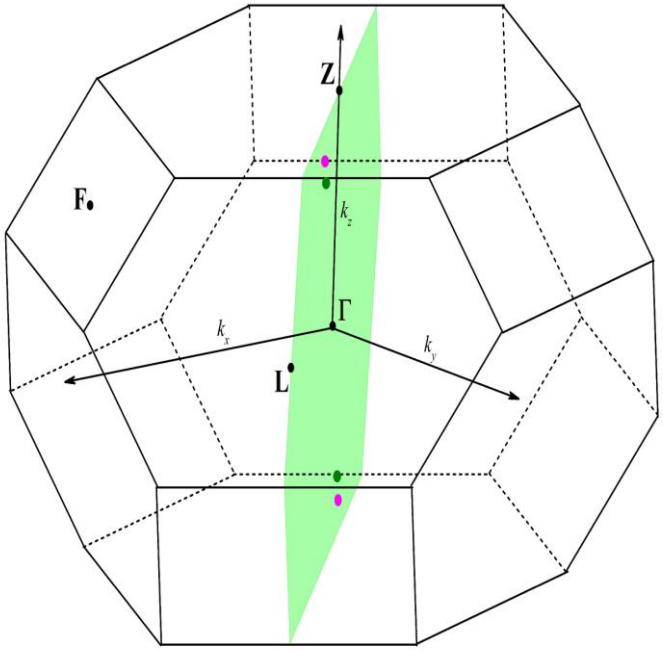

Figure S6. The graphical representation of the distribution of the symmetry protected Weyl points and the high-symmetry $k_x = k_y$ plane (highlighted in green).

The real-lattice ($\boldsymbol{a}_1$, $\boldsymbol{a}_2$, $\boldsymbol{a}_3$ for primitive cell and $\boldsymbol{b}_1$, $\boldsymbol{b}_2$, $\boldsymbol{b}_3$ for conventional cell, as marked in Fig. 1) can be expressed as

$$\begin{gathered}\boldsymbol{a}_1 = -\frac{a}{2}\hat{i} - \frac{\sqrt{3}}{6}a\hat{j} + \frac{c}{3}\hat{k},\ \boldsymbol{a}_2 = \frac{a}{2}\hat{i} - \frac{\sqrt{3}}{6}a\hat{j} + \frac{c}{3}\hat{k},\ \boldsymbol{a}_3 = \frac{\sqrt{3}}{3}a\hat{j} + \frac{c}{3}\hat{k}, \\ \boldsymbol{b}_1 = -\frac{a}{2}\hat{i} + \frac{\sqrt{3}}{2}a\hat{j},\ \boldsymbol{b}_2 = a\hat{i},\ \boldsymbol{b}_3 = c\hat{k}\end{gathered}, \quad (1)$$

The reciprocal-lattice vectors $\boldsymbol{t}_{1,2,3}$ are defined by $\boldsymbol{t}_i \cdot \boldsymbol{a}_j = 2\pi\delta_{ij}$, are given as

$$\boldsymbol{t}_1 = \frac{2\pi}{a}\left(-\hat{i} - \frac{\sqrt{3}}{3}\hat{j} + \frac{a}{c}\hat{k}\right),\ \boldsymbol{t}_2 = \frac{2\pi}{a}\left(\hat{i} - \frac{\sqrt{3}}{3}\hat{j} + \frac{a}{c}\hat{k}\right),\ \boldsymbol{t}_3 = \frac{2\pi}{a}\left(\frac{2\sqrt{3}}{3}\hat{j} + \frac{a}{c}\hat{k}\right), \quad (2)$$

Here $\hat{i}$, $\hat{j}$, and $\hat{k}$ represent the unit vector of k_x, k_y, and k_z in Cartesian coordanates, respectively. a and c are the optimized lattice parameters of conventional cell.

7. The Fermi surface map and the spin texture in the (001) plane

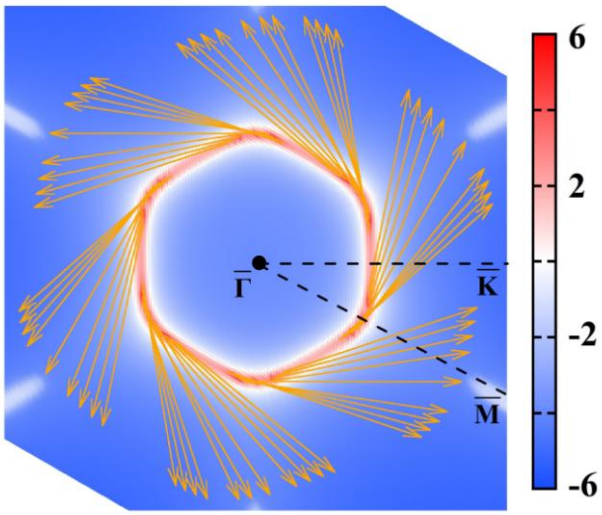

Figure S7. The Fermi surface mapped in the (001) plane as well as the spin texture at the energy of −0.1 eV.

8. Bands structures projected onto $k_x = k_y$ surface

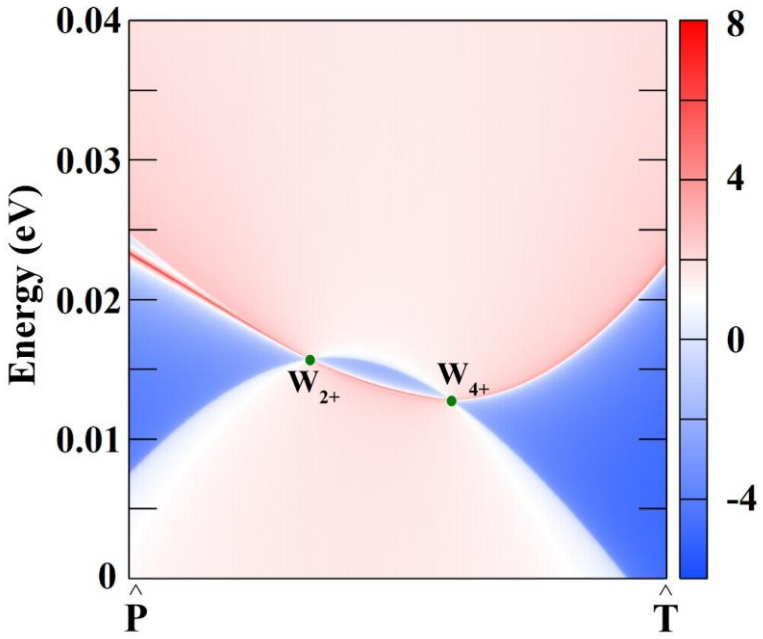

Figure S8. The $k_x = k_y$ plane surface state of $BiSbTe_3$ in $\hat{\mathbf{P}}-\hat{\mathbf{T}}$ line (Perpendicular to $\hat{\mathbf{\Gamma}}$-$\hat{\mathbf{R}}$ direction).

9. The coordinates of Weyl points under out-of-plane strains

Table R1. The coordinates in momentum space and the chirality of Weyl points in $k_x = k_y$ plane with 2% compressive and tensile strains along interlayer directions.

		Coordinate	Chirality
$c = 0.98\ c_0$	W_{1-}	(−0.411, −0.411, −0.324)	−1
	W_{1+}	(−0.394, −0.394, −0.307)	+1
	W_{3-}	(0.411, 0.411, 0.324)	−1
	W_{3+}	(0.394, 0.394, 0.307)	+1
$c = 1.02\ c_0$	W_{1-}	(−0.432, −0.432, −0.330)	−1
	W_{1+}	(−0.412, −0.412, −0.310)	+1
	W_{3-}	(0.432, 0.432, 0.330)	−1
	W_{3+}	(0.412, 0.412, 0.310)	+1

10. The evolution lines of Wannier centers for $BiSbTe_3$ with strains

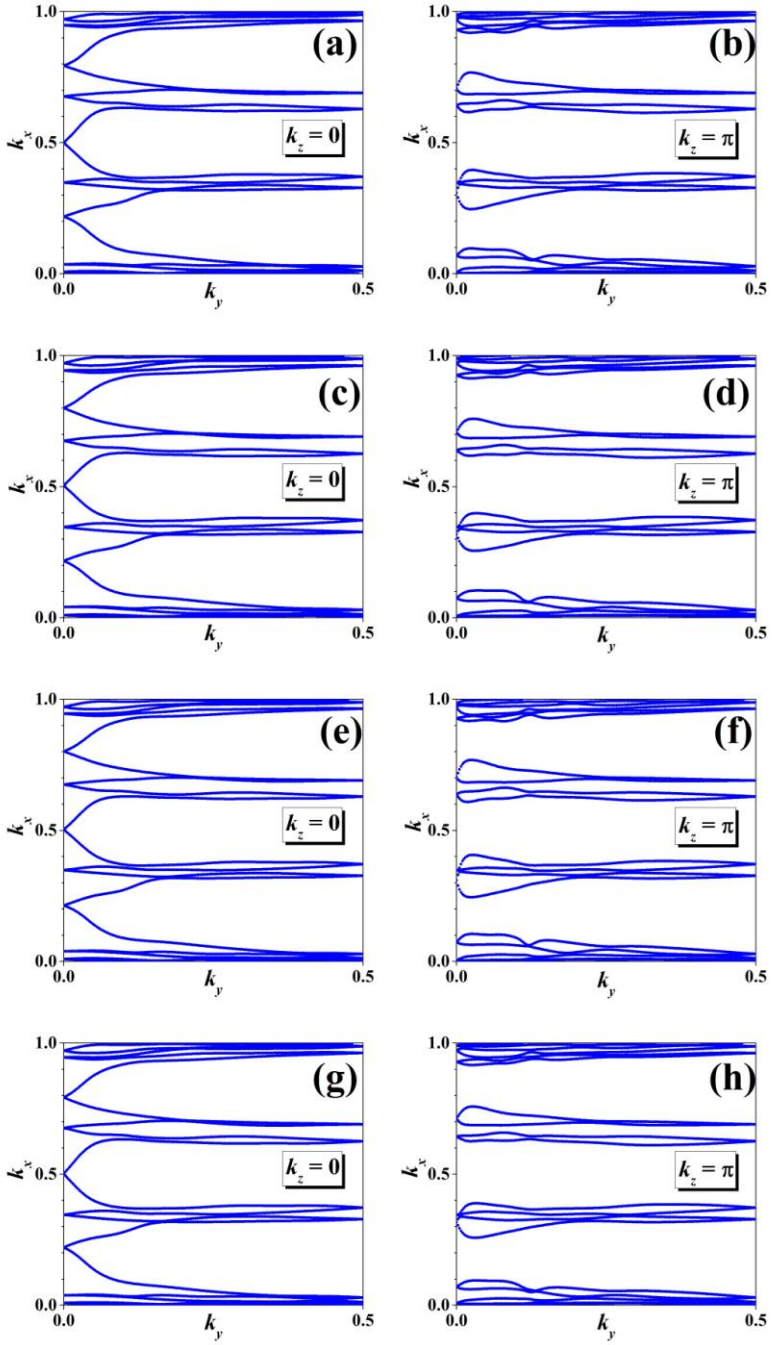

Figure S9. Calculated evolution lines of Wannier centers in $\boldsymbol{k_z} = 0$ and $\boldsymbol{k_z} = \pi$ planes under (a)~(b) 2% in-plane compressive strains, (c)~(b) 2% in-plane tensile strains, (e)~(f) 2% out-of-plane compressive strains, and (g)~(h) 2% out-of-plane tensile strains.